Chemical Sciences Journal
ISSN: 2150-3494

Mustafa et al., Chem Sci J 2019, 10:1
DOI: 10.4172/2150-3494.1000199

Research Article Open Access

# The Mechanism, Kinetic Study and Non-Linear Optical Properties (NLO) of Para-Chloroaniline Using DFT Approach

**Mustafa HM[1*], Khaliel AB[2] and Ali MY[3]**
[1]Department of Chemistry, Faculty of Science, Cairo University, Egypt
[2]Department of Chemistry, Faculty of Science, Beni Suef University, Egypt
[3]Department of Basic Science, Canadian International College (CIC), Egypt

**Abstract**

The synthesis of poly-p-chloroaniline (PpCA) by oxidative chemical polymerization using potassium dichromate as oxidizing agent was carried out. The optimum conditions for the polymerization reaction and the order of reactions and thermodynamic activation parameters were investigated. A molecular mechanism for the oxidation of p-chloroaniline using potassium dichromate is proposed. The TGA analysis and spectroscopic studies IR, UV-vis and elemental analysis have evidenced the structure of polymeric chain. The surface morphology of the obtained polymer was characterized by X-ray diffraction and transmission electron microscopy (TEM). Moreover, determinations of dielectric properties of the prepared polymer were carried out. The a.c conductivity ($\sigma_{ac}$) of (PpCA) was investigated as a function of frequency and temperature. The microscopic conduction mechanism of charge carries over the potential barrier in polymer backbone was found classical hopping model. The electronic structure of neutral PpCA, radical cation and dimer radical cation are investigated theoretically at the B3LYP/6-311G** level of theory. The mechanism of the polymerization process is discussed and analyzed. The calculated EHOMO and ELUMO energies of the studied compounds can be used to calculate the global properties; chemical hardness (η), softness (S) and electronegativity (χ). The calculated nonlinear optical parameters (NLO); polarizibilty (α), anisotropy of the polarizibility (Δα) and first order hyperpolarizibility (β) of the studied compounds show promising optical properties. 3D-plots of the molecular electrostatic potential (MEP) for neutral monomer and radical cation dimer are investigated and analyzed showing the distribution of electronic density of orbitals describing the electrophilic and nucleophilic sites of the neutral monomer and radical cation dimer.

**Keywords:** Oxidative chemical polymerization; p-Chloroaniline characterization; Kinetics; Electrical conductivity; DFT calculations; NLO properties

## Introduction

Conducting polymers have been extensively studied due to their interesting electrical and electrochemical properties. Polyaniline (PANI) is one of the most studied conducting polymers due to its simple synthesis method [1]. It has various potential applications in many high-performance devices [2-8]. A common feature of conducting polymer is conjugation of $\pi$-electrons extending over the length of the polymer backbone [9]. Polymerization of conducting polymer may be performed by chemical or electrochemical methods [10,11]. Kinetics of the oxidation of p-Chloroaniline, m-Chloroaniline and p-Chloroaniline using Fe (III) as oxidant and 1,10-Phenanthroline as catalyst were investigated spectrophotometrically, the reaction obeys first order kinetics both in the substrate and iron (III) [12]. Plots of $1/k_1$ versus $1/[catalyst]^2$, $1/k_1$ $[H^+]$ versus $[H^+]^2$ and $1/k_1$ versus $[HSO^-_4]^2$ are linear with positive intercepts on the $1/k_1$ axis in each case. The stability constant of the complex formed between Fe (III) and catalyst and the activation parameters have been evaluated. A suitable mechanism has been proposed. Three principal ways to synthesize the polychloroanilines such as chemically oxidative solution polymerization, chemically oxidative emulsion polymerization and electrochemical polymerization are concluded. The resulted polychloroanilines possess-conjugated structures like polyaniline backbones. And the presence of chloro-substituted groups accounts for excellent solubility and sensitive electrocatalysis. The polychloroanilines are of stronger catalysis sensitivity and higher stability in modified electrode than inorganic compounds and other conducting polymers. They are new functional materials with great development potential. They can be applied in a wide area such as modified electrode, pH sensor and gas separation membrane [13]. To understand the orientation effect of polychloroaniline on the electrophilic substitution, the charges of carbon atoms in the benzene ring and the energy of σ complexes formed in the electrophilic substitution were computed by B3LYP at 6-311G** level, according to density functional theory (DFT). Results showed that ortho-and para-chlorines were preferentially substituted instead of meta-chlorines, because the charges of ortho-and para-carbon atoms, the energy of ortho-and para-σ complexes were less than that of meta [14]. The aniline derivatives which prepared chemically are almost all donating substitution on benzene ring as (alkyloxy, hydroxy, chloroaniline, etc.) and also at the nitrogen atom was reported by Sayyah et al. [15] to improve the solubility of polyaniline, The kinetics of chemical polymerization of 3-methylaniline, 3-chloroaniline, 3-hydroxyaniline, 3-methoxyaniline and N-methyl aniline in hydrochloric acid solution using potassium dichromate as oxidant and characterization of the polymer obtained by IR, UV-visible and elemental analysis, X-ray diffraction, scanning electron microscopy, TGA-DTA analysis and a.c conductivity have been reported by Sayyah et al. [15-23].

In the literature, there is no systematic study of the structure mechanism and nonlinear properties. Such study is important for understanding the industrial application and NLO properties of these molecules [24-51]. Non-linear optical properties (NLO) are the ability of any compound to convert light [with intense electric field (LASER)] of longer wave length into light of shorter wave length. One of the non-linear optical phenomena is the second harmonic generation (SHG)

***Corresponding author:** Mustafa HM, Department of Chemistry, Faculty of Science, Cairo University, Cairo, Egypt, Tel: +201025783555; E-mail: mali2007@hotmail.com

**Received** February 10, 2019; **Accepted** February 28, 2019; **Published** March 12, 2019

**Citation:** Mustafa HM, Khaliel AB, Ali MY (2019) The Mechanism, Kinetic Study and Non-Linear Optical Properties (NLO) of Para-Chloroaniline Using DFT Approach. Chem Sci J 10: 199. doi:10.41722380-2391.1000199

where intense light of longer wave length is converted to half of the incident value, upon absorption by the non-linear optical material as shown in Figure 1.

## Aim of the Work

The present works study the kinetics of the oxidative chemical polymerization using potassium dichromate as oxidant for p-chloroaniline monomer in aqueous HCl medium. The obtained polymer is characterized by IR, UV-visible, TGA, elemental analysis, X-ray, transmission electron microscopy (TEM) and a.c conductivity measurements. The mechanism of the polymerization process is investigated theoretically using DFT-B3LYP/6-311G**. The electronic dipole moment (μ) and first order hyperpolarizibility (β) values of the monomer, radical cation and dimer cation have been computed to study the NLO properties. Finally, global reactivity descriptors including electronegativity (X), hardness (η), softness (S) of the monomer, radical cation and dimer cation were calculated and analyzed, while molecular electrostatic potential (MEP) of some selected molecules were explored as well.

## Experimental

### Materials

P-Chloroaniline provided by Honeywell Chemical Co., (Germany). Concentrated hydrochloric acid, pure grade product, provided by El-Nasr pharmaceutical chemical Co., Egypt. Potassium dichromate provided by Sigma-Aldrich chemical Co., (Germany). Doubly distilled water was used to prepare all the solutions needed in the kinetic studies.

### Oxidative aqueous polymerization of p-chloroaniline monomer

The polymerization reaction was carried out in a well-stoppered conical flask of 100 ml capacity; addition of PCA amount in 15 ml HCl (as dopant and acid medium) of known molarity followed by the addition of the required amount of potassium dichromate as oxidant (2 M) in water (10 ml) to the reaction mixture, the total volume of the reaction mixture is constant at 25 ml at 15°C for one hour). The orders of addition of substances were kept constant in all the performed experiments. The stoppered conical flasks were then placed in an automatically controlled thermostat at the required temperature. The flasks were shaken (15 shakings/10 s/30 min) by using an automatic shaker. The flasks were filtrated using a Buchner funnel, and then the obtained polymer was washed with distilled water, and finally dried till constant weight in vacuum oven at 60°C until constant weight.

### Elemental analysis, infrared and ultraviolet spectroscopy

The carbon, hydrogen and nitrogen contents of the prepared polymer were carried out in the micro analytical laboratory at Cairo University by using oxygen flask combustion and a dosimat E415 titrator (Switzerland).

The infrared spectroscopic analysis of the prepared polymer was carried out in the micro analytical laboratory at Cairo University by using a Shimadzu FT/IR-4600 Jasco spectrophotometer {Standard wavenumber measurement range: 7,800 to 350 $cm^{-1}$, (Optional extended wavenumber range: 15,000 to 2,200 $cm^{-1}$-5,000 to 220 $cm^{-1}$), Maximum resolution: 0.7 $cm^{-1}$ and rapid scan: 10 Hz (optional)} by using KBr disc technique for the IR investigations. The ultraviolet-visible absorption spectra of the monomer and the prepared polymer sample were measured using Shimadzu UV spectrophotometer (1600 Series) at room temperature in the range 200-400 nm using dimethylformamide as a solvent and reference.


**Figure 1:** Second-order non-linear crystal.

### Thermal gravimetric analysis (TGA), Transmission electron microscopy (TEM) and X-ray analysis

Thermal gravimetric analysis (TGA) of the polymer sample was performed using a TGA-51 SHIMADZU Thermogravimetric Analyzers analyzer. The weight loss was measured from ambient temperature up to 600°C, at rate of 20°C/min to determine the rate of degradation of the polymer. The start weight 1.666 g we calculate the weight loss=$M_1$-$M_0$, where $M_1$ is the weight at Temperature (T) and $M_0$ is the start weight, where the percentage of the loss weight (%) is given on the figure from Analysis Center. So, we defined the loss molecules according to molecular weight.

X-Ray diffractometer (Philip 1976 model 1390) was used to investigate the phase structure of the polymer powder under the following condition which kept constant during the analysis processes: Cu, -X-ray tube, -scan speed=8/min, - current=30 mA, -voltage=40 kv and preset time=10 s. The inner cavity and wall thickness of the prepared polymer was investigated using transmission electron microscopy (TEM) JEOL JEM-1200 EX II (Japan).

### Dielectric properties and a.c conductivity measurements

The dielectric constant (έ), the dielectric loss (ε") and Ac conductivity $\sigma_{ac}$ were measured using Philips RCL bridge (digital and computerized) at a frequency range 12-$10^5$ Hz and over temperature range 30-60°C.

The values of the dielectric constant were determine using standard geometric technique in which the capacitance (C) was assumed to be given by the usual expression for a parallel plate capacitor i.e., using formula:

$$\varepsilon' = \frac{Cd}{\varepsilon_0 A} \quad (1)$$

where έ is the dielectric constant, $\varepsilon_o$ is the permittivity of vacuum, A is the area of the sample and d is the sample thickness.

The dielectric loss ε" was calculated from the measurements of the loss factor D and έ using the following relation:

$$\varepsilon'' = D\varepsilon \quad (2)$$

The Ac conductivity was measured using Philips RCL Bridge (digital and computerized) at a frequency range 0.1-100 k Hz and at temperature range 30-80°C. The temperature was controlled by the use of a double wound electric oven.

The ac conductivity $\sigma_{ac}$ value was calculated using the relation:

$$\sigma_{ac} = \varepsilon'' \omega \varepsilon_0 \quad (3)$$

where ω=2πf and f is the applied frequency.

### Calculations

**Determination of conversion yield:** The conversion yield of the monomer to the polymer was determined by the weighing of the dry obtained polymer (P) divided by the weight of the monomer (w) and

was calculated in the following way:

$$\text{Conversion yield} = \frac{\text{Polymer Yield(P)}}{\text{Weight of Momoner (w)}} \quad (4)$$

**Determination of the polymerization rate: The rate of polymerization was determined in the following:**

$$\text{Rate}(R_i) = \frac{P}{V \times M.wt \times t} (\text{gmol/L.sec}) \quad (5)$$

where P is the weight of polymer formed at time (t) in seconds, V is the volume of the reaction solution in liters and m. wt. is the molecular weight of the monomer [22].

**Calculation of the apparent energy of activation:** The apparent activation energy (Ea) of the aqueous polymerization reaction was calculated using the following Arrhenius equation:

$$Log(K) = \frac{-Ea}{2.303RT} + C \quad (6)$$

where K is the rate, R is the universal gas constant, T is the reaction temperature and C is constant [23].

**Determination of enthalpy ($\Delta H^*$) and entropy ($\Delta S^*$):** Enthalpy of activation ($\Delta H^*$) and entropy ($\Delta S^*$) were calculated using transition state theory equations (Eyring equation):

$$K = \frac{RT}{Nh} e^{\Delta S^*/R} \cdot e^{-\Delta H^*/RT} \quad (7)$$

where K is the rate constant, N is the Avogadro's number, R is the universal gas constant and h is Planck's constant.

By dividing the above equation by T and taking its natural logarithm we obtain the following equation:

$$Ln\left(\frac{K}{T}\right) = Ln\frac{R}{Nh} + \frac{(\Delta S^*)}{R} + \frac{(-\Delta H^*)}{RT} \quad (8)$$

A plot of Ln (K/T) against 1/T is linear, with a slope equals to ($-\Delta H^*/R$) and intercept equals to ($LnR/Nh+\Delta S^*/R$). Therefore $\Delta H^*$ and $\Delta S^*$ can be calculated from the slope and intercept, respectively [22,23].

## Computational methods

All computations were carried out using Gaussian 09 W hyperchem 8.0, chemcraft 1.6, Gaussview 9.0 and is draw software package. Molecular geometries of all the studied compounds were fully optimized using B3LYP/6-311G** [24-28]. No symmetry constrains were applied during the geometry optimization [29,30]. The choice of this basis set was due to its flexibility and the fact that the diffused p functions on the H-atom tend to compensate the inharmonic effects of the CH and NH stretches. By using HOMO and LUMO energy values for a molecule, using RHF/6-311G**, electronegativity and chemical hardness can be calculated as follows: X=(I+A)/2 (electronegativity), η=(I-A)/2 (chemical hardness), S=1/2η (chemical softness) where I and A are ionization potential and electron affinity, and $I=-E_{HOMO}$ and $A=-E_{LUMO}$, respectively [31,32]. Throughout this work MOs were constructed using the Gauss-view 5.08 visualization program [33]. The total static dipole moment (μ), the mean polarizability <α>, the anisotropy of the polarizability Δα and the mean first hyper polarizability <β> using the x, y, z components were calculated by using the following equations [34,35]:

$$\mu = \left(\mu_X^2 + \mu_Y^2 + \mu_Z^2\right)^{1/2}$$

$$\alpha = \frac{(\alpha xx + \alpha yy + \alpha zz)}{3}$$

$$\Delta\alpha = \sqrt{\frac{(\alpha xx - \alpha yy)2 + (\alpha yy - \alpha zz)2 + (\alpha zz - \alpha xx)2}{2}}$$

$$<\beta> = \sqrt{\beta_{X^2} + \beta_{y^2} + \beta_{z^2}}$$

Where:

$b_x = b_{xxx} + b_{xyy} + b_{xzz}$

$b_y = b_{yyy} + b_{xxy} + b_{yzz}$

$b_z = b_{zzz} + b_{xxz} + b_{yyz}$

## Results and Discussion

### Determination of the optimum polymerization conditions

**Effect of HCl concentration:** The effect of HCl concentration on the aqueous oxidative chemical polymerization of p-chloroaniline (pCA) is investigated using constant concentrations for both of $K_2Cr_2O_7$ and monomer at 0.2 M by using different concentrations of HCl at 15°C ± 0.2 for one hour. The yield-time curve is represented in Figure 2, from which it is clear that the obtained yield increases with the increase of HCl concentrations in the range from 0.1 M to 0.5 M then decreases gradually till 0.65 M.

**Effect of the monomer concentration:** The effect of monomer concentration on the aqueous oxidative chemical polymerization of P-chloroaniline (pCA) is investigated using constant concentration of $K_2Cr_2O_7$ at 0.2 M and HCl concentration at 0.5 M by using different concentrations of P-chloroaniline (pCA) at 15°C ± 0.2 for one hour. The yield-time curve is represented in Figure 3, from which it is clear that the obtained yield increases with the increasing of P-chloroaniline concentrations in the range from 0.1 M to 0.2 M then decreases gradually to 0.5 M.

**Effect of potassium dichromate concentration:** Both of the monomer and HCl concentrations are kept constant at 0.2 M and 0.5 M respectively while the oxidant concentrations are varied from 0.1 M to 0.5 M at 15°C ± 0.2 for one hour to investigate the optimum polymerization condition of the oxidant. Figure 4 shows the plot of polymer yield of (pCA) against different concentrations of the oxidant. The obtained yield increases with the increase of $K_2Cr_2O_7$ concentration reaching maximum value at 0.3 M then decreases from 0.3 M to 0.5 M. In the first part of the curve the produced initiator ion radical moieties activate the

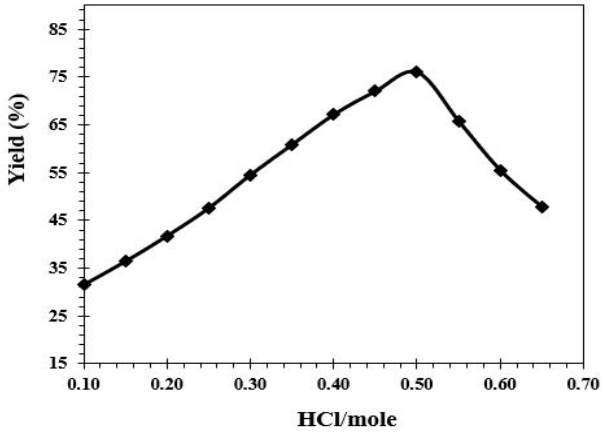


**Figure 2:** Effect of HCl concentrations on the aqueous oxidative chemical polymerization of (pCA).

backbone and consequently produce the p-chloroaniline (pCA) radical cation, which takes place immediately and therefore, the yield increases with the increase of potassium dichromate concentration up to 0.3 M. But in the range from 0.3 M to 0.5 M the polymer yield decreased. This could be attributed to the higher concentration of oxidant (more than 0.3 M) lead to the formation of low molecular weight oxidation product which is easily soluble in acid medium [23,36].

## The kinetic studies of the polymerization reaction

**Effect of HCl concentration:** The kinetic study of the aqueous oxidative chemical polymerization for (PCA) is carried out using constant monomer concentration at 0.2 M and $K_2Cr_2O_7$ as oxidant at (0.3 M) using different molarities of HCl 0.1-0.5 mole/L and using constant total volume (25 ml) at 15°C ± 0.2 for different time intervals. The data are tabulated in Table 1 and the yield-time curves are graphically represented in Figure 5. From which, it is clear that, both the initial and overall reaction rates of the polymerization reaction increase with the increasing of HCl concentrations in the range between 0.1-0.5 mole/L. The HCl exponent is determined from the relation between the logarithms of the initial rate of polymerization log ($R_i$) against logarithm of the HCl concentration log [HCl] as represented in Figure 6. A straight line is obtained with a slope equal to 1.017, which means that the polymerization reaction is a first order reaction with respect to HCl concentration.

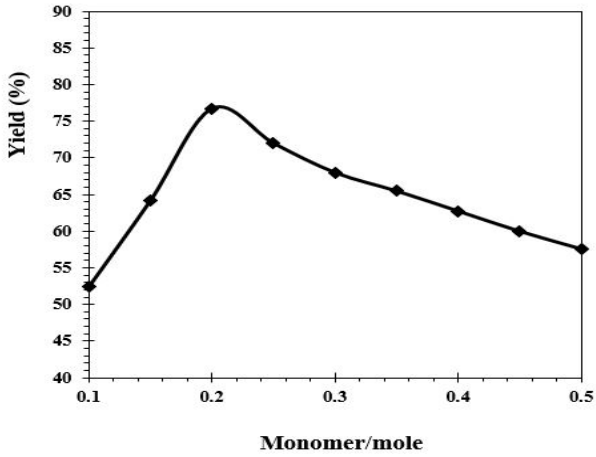


**Figure 3:** Effect of monomer concentrations on the aqueous oxidative chemical polymerization of (pCA).

**Effect of potassium dichromate concentration:** The effect of $K_2Cr_2O_7$ on the aqueous chemical oxidative polymerization of (pCA) is carried out at fixed concentrations of monomer at 0.2 M and HCl at 0.5 M. The oxidant concentration is investigated in the range between 0.05-0.3 mole/L using constant total volume (25 ml) at 15°C ± 0.2 for different time intervals. The data are tabulated in Table 2 and the yield-time curves are graphically represented in Figure 7 which shows that, both of the initial and overall reaction rate of the polymerization reaction increase with the increasing of oxidant concentration in the range between 0.05-0.3 mole/L. The oxidant exponent is determined from the relation between logarithms of the initial rate of polymerization log ($R_i$) against logarithm of the oxidant concentration [$K_2Cr_2O_7$]. A straight line is obtained with a slope of 0.934 as given in Figure 8. This means that the polymerization reaction of (pCA) is a first order reaction with respect to the oxidant.

**Effect of monomer (pCA) concentration:** The effect of monomer concentration on the aqueous oxidative chemical polymerization of pCA is investigated by using different concentrations of monomer (0.05-0.2 mole/L) at constant volume (25 ml). The HCl solution and potassium dichromate concentrations are fixed at 0.5 M and 0.3 M respectively at 15°C ± 0.2 for different time intervals. The data are tabulated in Table

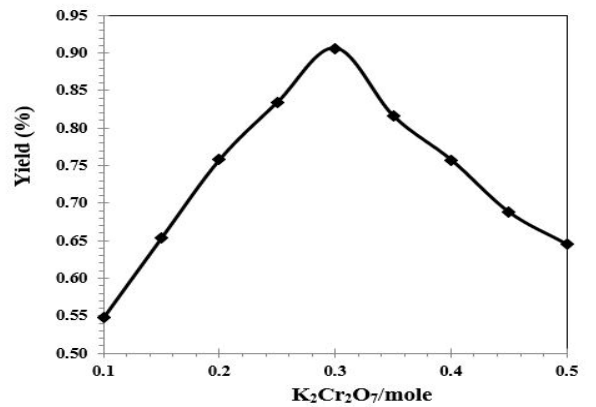


**Figure 4:** Effect of $K_2Cr_2O_7$ concentrations on the aqueous oxidative chemical polymerization of (PCA).

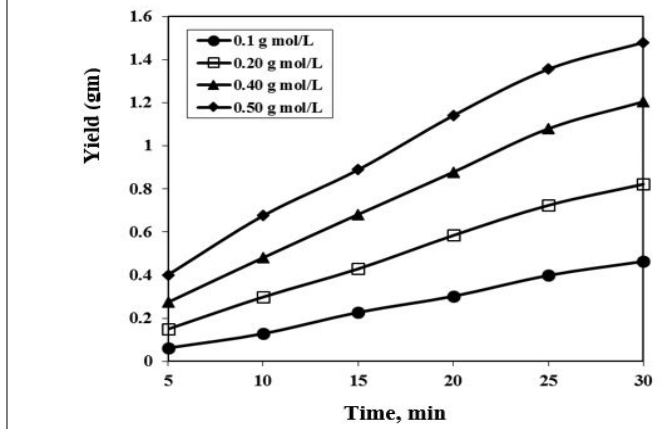


**Figure 5:** Yield-time curves for the effect of HCl concentrations on aqueous oxidative chemical Polymerization of (pCA) at different time intervals.

| No. | HCl (M) | Yield (gm) Time (min) | | | | | | Rate of polymerization mole. $L^{-1}$ .$sec^{-1}$ | |
|---|---|---|---|---|---|---|---|---|---|
| | | 5 | 10 | 15 | 20 | 25 | 30 | Initial × $10^{-5}$ | Overall × $10^{-5}$ |
| 1 | 0.1 | 0.06 | 0.13 | 0.21 | 0.3 | 0.4 | 0.48 | 6.79 | 8.15 |
| 2 | 0.2 | 0.19 | 0.3 | 0.44 | 0.58 | 0.72 | 0.85 | 15.68 | 15.26 |
| 3 | 0.4 | 0.29 | 0.48 | 0.68 | 0.89 | 1.08 | 1.24 | 31.36 | 22.99 |
| 4 | 0.5 | 0.45 | 0.68 | 0.9 | 1.14 | 1.36 | 1.52 | 41.81 | 29.26 |

**Table 1:** Effect of HCl concentration on the aqueous oxidative polymerization of pCA.

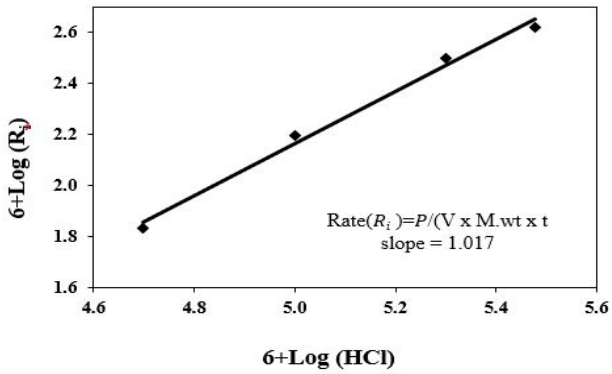


**Figure 6:** Double logarithmic plot of the initial rate and HCl concentration for aqueous oxidative chemical polymerization of (pCA).

| No | Oxidant (M) | Yield (gm) | | | | | | Rate of polymerization mole. $L^{-1}$ .$sec^{-1}$ | |
|---|---|---|---|---|---|---|---|---|---|
| | | Time (min) | | | | | | | |
| | | 5 | 10 | 15 | 20 | 25 | 30 | Initial × $10^{-5}$ | Overall × $10^{-5}$ |
| 1 | 0.05 | 0.06 | 0.15 | 0.26 | 0.39 | 0.52 | 0.64 | 7.68 | 10.82 |
| 2 | 0.1 | 0.18 | 0.33 | 0.5 | 0.68 | 0.87 | 1.03 | 17.25 | 18.15 |
| 3 | 0.2 | 0.32 | 0.5 | 0.71 | 0.93 | 1.14 | 1.32 | 28.22 | 23.77 |
| 4 | 0.3 | 0.45 | 0.68 | 0.9 | 1.14 | 1.36 | 1.52 | 41.81 | 28.36 |

**Table 2:** Effect of $K_2Cr_2O_7$ concentrations on the polymerization of (pCA).

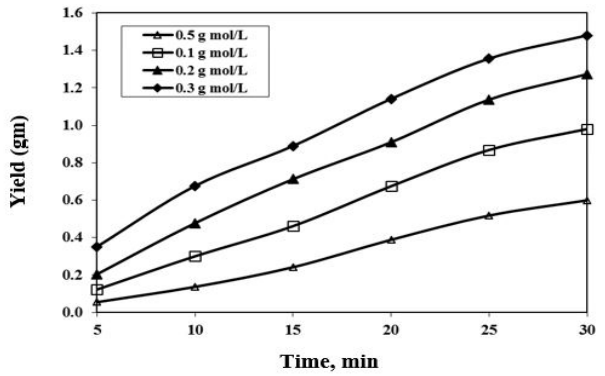


**Figure 7:** Yield-time curves for the effect of oxidant concentrations on aqueous oxidative chemical polymerization of (pCA) at different time intervals.

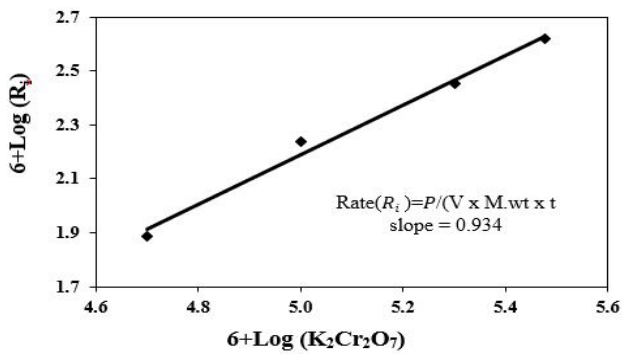


**Figure 8:** Double logarithmic plot of the initial rate and oxidant concentrations for aqueous oxidative chemical polymerization of (pCA).

3 and the yield-time curves are plotted for the investigated monomer concentrations in Figure 9. The monomer exponent is determined from the slope of the straight line represented in Figure 10 for the relation between log ($R_i$) and logarithm of the monomer concentration [M]. The slope of this linear relationship is found to be 1.142 which means that the polymerization reaction is a first order reaction with respect to the monomer concentration.

## Calculation of the thermodynamic activation parameters

The aqueous oxidative chemical polymerization of 0.20 mole/L (pCA), 0.5 mole/L HCl and 0.3 mole/L potassium dichromate as oxidant is carried out at different temperatures (5, 10 and 15°C) for different time intervals. The yield- time curves are plotted in Figure 11. From which, it is clear that both of the initial and overall reaction rates increase with the raising of the reaction temperature. The apparent activation energy (Ea) of the aqueous oxidative chemical polymerization reaction is calculated

| No | Monomer (M) | Yield (gm) Time (min) | | | | | | Rate of polymerization mole. $L^{-1}$ .$sec^{-1}$ | |
|---|---|---|---|---|---|---|---|---|---|
| | | 5 | 10 | 15 | 20 | 25 | 30 | Initial × $10^{-5}$ | Overall × $10^{-5}$ |
| 1 | 0.05 | 0.03 | 0.09 | 0.15 | 0.22 | 0.3 | 0.38 | 4.75 | 6.27 |
| 2 | 0.1 | 0.07 | 0.18 | 0.31 | 0.45 | 0.6 | 0.75 | 9.51 | 12.54 |
| 3 | 0.15 | 0.2 | 0.37 | 0.56 | 0.75 | 0.95 | 1.12 | 19.86 | 19.86 |
| 4 | 0.2 | 0.45 | 0.68 | 0.9 | 1.14 | 1.36 | 1.52 | 41.81 | 28.43 |

**Table 3:** Effect of monomer concentrations on the polymerization of (pCA).

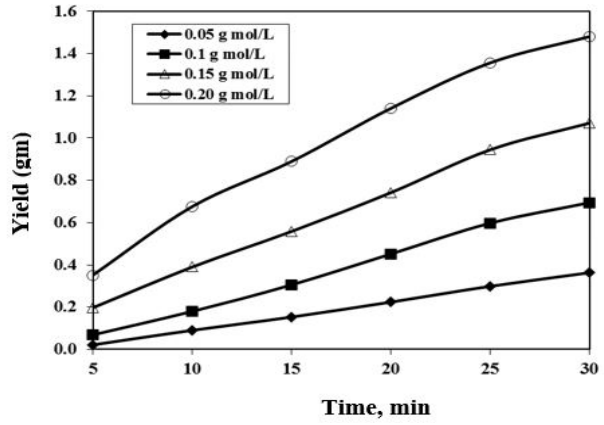


**Figure 9:** Yield-time curves for the effect of monomer concentrations on aqueous oxidative chemical polymerization of (pCA) at different time intervals.

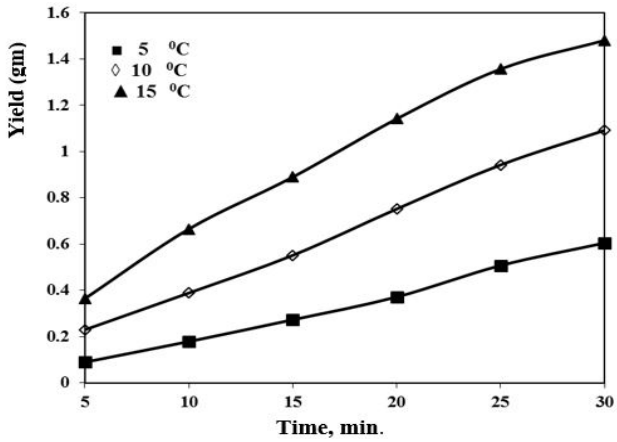


**Figure 11:** Yield-time curve for the effect of temperature on the aqueous oxidative chemical polymerization of (pCA).

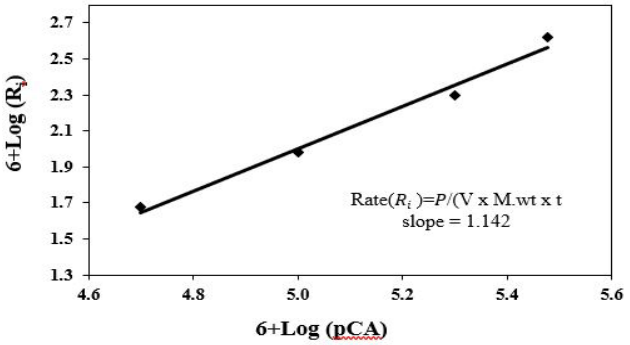


**Figure 10:** Double logarithmic plot of the initial rate and monomer concentration for aqueous oxidative chemical polymerization of (pCA).

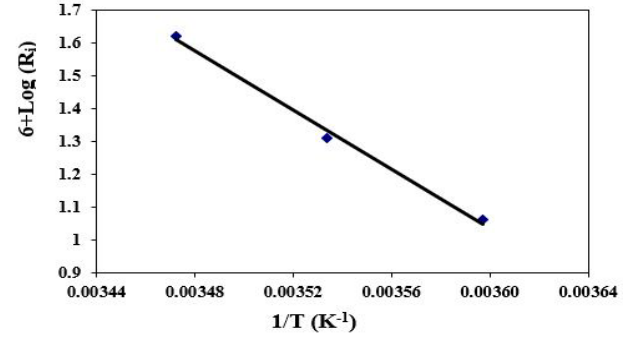


**Figure 12:** The relation between the logarithm of initial rate and (1/T) for the aqueous chemical oxidative polymerization of (pCA).

using equation (6). The apparent activation energy for this system is found to be 85.61 kJ/mole. The enthalpy and entropy of activation for the polymerization reaction can be calculated by the calculation of K from the following equation [22,37]:

Reaction Rate=K[oxidant] 0.934 [HCl] 1.017 [monomer] 1.142 (9)

The values of K at 5, 10 and 15°C are $2.07 \times 10^{-6}$, $4.32 \times 10^{-6}$ and $7.89 \times 10^{-6}$ respectively. The enthalpy ($\Delta H^*$) and entropy ($\Delta S^*$) of activation associated with K, are calculated using Eyring equation:

$K=(RT/Nh)\, e^{\Delta S^*/R}.\, e^{-\Delta H^*/RT}$

where K is the rate constant, N is the Avogadro's number, R is the universal gas constant and h is Planck's constant (Figure 12).

Figure 13 shows the relation between K/T vs 1/T, which gives a linear relationship with a slope equal to $(-\Delta H^*)/R$ and intercept equal

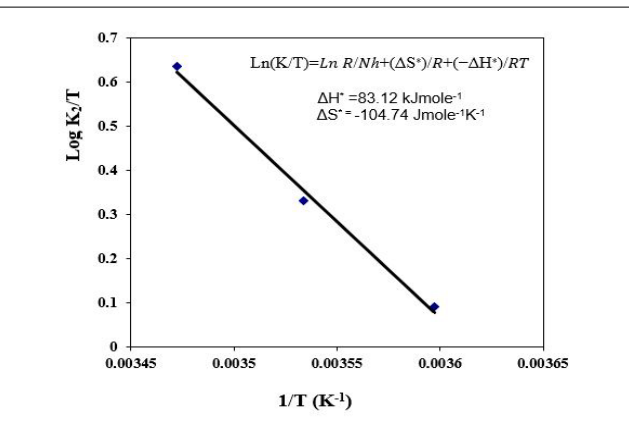


**Figure 13:** The relation between log $K_2/T$ and 1/T for the polymerization reaction of (pCA).

to (log R/Nh+$\Delta S^*$/R). From the slope and intercept, the values of $\Delta H^*$ and $\Delta S^*$ are calculated and are found to be equal to 83.12 kJmole$^{-1}$ and -104.74 J mole$^{-1}$K$^{-1}$ respectively.

## Polymerization mechanism

The Mechanism of the Aqueous Oxidative Chemical Polymerization of P-Substituted Aniline Derivatives (PSAD): Oxidative chemical polymerization is often considered as a kind of poly condensation, since chain growth is accompanied by the formation of low-molecular products. The formation of chain may proceed in two ways. The first one is recombination of cation radical oxidation sites. In this case, polymer growth process is classed as poly condensation and the second way of chain growth belongs to electrophilic substitution; in the case of substituted-aniline, oxidized nitrogen-containing structure attacks phenyl ring of another aniline molecule and substitute one proton of the ring. The ring and nitrogen-containing structure lose one proton; after that, monomer units bind with each other and the chain becomes longer [23,36] (Scheme 1). The aqueous oxidative polymerization of P-choloro aniline derivatives is described as follows in three steps [23,36].

**The initial step:** Potassium dichromate in acidified aqueous solution produces chromic acid as shown in equation 10:

$$K_2Cr_2O_7+H_2O+2H^+\rightarrow 2K^++2H_2CO_4 \quad (10)$$

This reaction is controlled by the change in pH, the orange red dichromate ions $(Cr_2O_7)^{2-}$ are in equilibrium with the $(HCrO_4)^-$ in the range of pH-values between 2 and 6, but at pH below 1 the main species is $(H_2CrO_4)$ and the equilibrium can occur as follows:

$$(HCrO_4)^- \rightleftharpoons (CrO_4)_{2-}+H^+ \qquad K=10\text{-}5.9 \quad (11)$$

$$(H_2CrO_4) \rightleftharpoons (HCrO_4)^-+H^+ \qquad K=4.1 \quad (12)$$

$$2(HCrO_4)^- \rightleftharpoons (Cr_2O_7)^{2-}+H_2O \qquad K=10\text{-}2.2 \quad (13)$$

The chromic acid withdraws one electron from each protonated P-choloro aniline and probably forms a metastable complex as shown in equation 14:

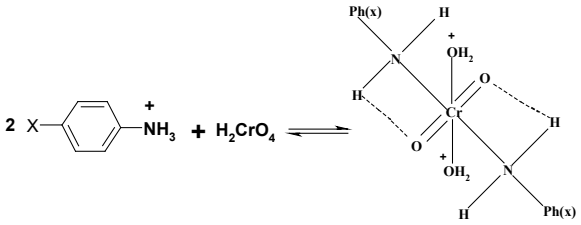


(14)

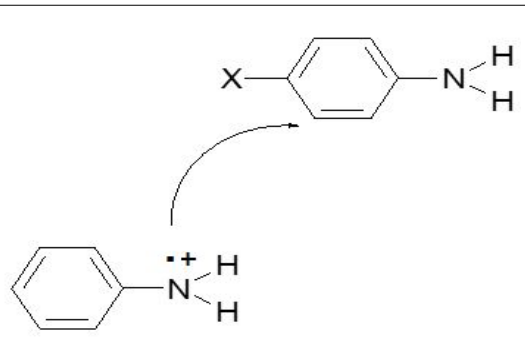


**Scheme 1:** Electrophilic substitution reaction.

Where, X=Cl

The complex undergoes dissociation to form monomer cation radical as shown in equation 15:

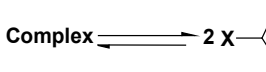


(15)

Generally, the initial step is rapid and may occur in short time, 0-5 min (autocatalytic reaction).

**Propagation step:** This step involves the interaction between the formed radical cation and the monomer to form a dimer radical cation. In the case of Cr (VI) oxidation of the organic compounds, Cr (VI) is reduced to Cr (IV) first and then to Cr (III) [36]. Transfer of two electrons from two monomer ion radical by $H_2CrO_4$ produces meta semidine salt along with chromous acid $H_2Cr_2O_3$ (Cr (IV)). The intermediately produced Cr (IV) oxidizes meta semidine to pernigraniline salt (PS) at suitable low pH and the PS acts as a catalyst for conversion of radical cation to polymer.

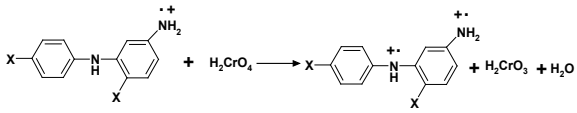


(16)

Para semidine (PS)

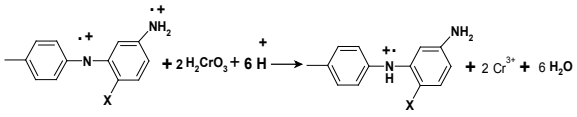


(17)

Pernigraniline salt

where, X=Cl

This reaction is followed by further reaction of the formed dimer radical cation with monomer molecules to form trimmer radical cation and so on. The degree of polymerization depends on different factors such as dichromate concentration, HCl concentration, monomer concentration, and temperature. By adding equations 10 and 14-17+

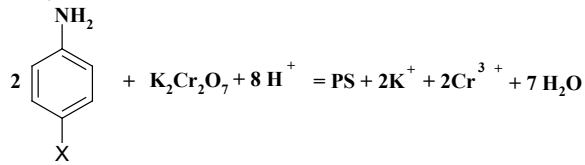


(18)

$$12\ (PSAD)+5K_2Cr_2O_7+34\ H^+=6\ PS+10Cr_3^++10K^++35\ H_2O \quad (19)$$

**Termination step:** Termination of the reaction occurs by the addition of ammonium hydroxide solution in an equal molar amount to HCl present in the reaction medium (till pH=7), which leads to cessation of the redox reaction. The reaction could occur as follows:

## Characterization of the obtained polymer

**The elemental analysis:** The data obtained from elemental analysis using oxygen flask combustion and a dosimat E415 titrator shows that, the found carbon content of (PpCA) is lower than the calculated value (Table 4). This is due to the formation of chromium carbide during step of heating and measuring process while the found value of nitrogen and hydrogen are 8.87 and 4.23 respectively which are in good agreement with the calculated one for the suggested structure present in Scheme

| C % | | N % | | H % | | Cl % | |
|---|---|---|---|---|---|---|---|
| Calc. | Found | Calc. | Found | Calc. | Found | Calc. | Found |
| 48.86 | 40.48 | 9.50 | 8.87 | 4.11 | 4.23 | 30.12 | 28.93 |

**Table 4:** The elemental analysis of PpCA.

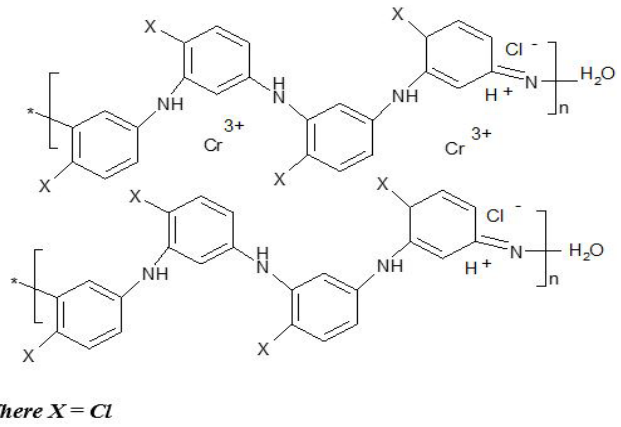


**Scheme 2:** Structure of the prepared poly p-chloroaniline (PpCA).

2. By measuring another sample of the (PpCA) which was prepared by using ammonium persulfate as oxidant the found value of carbon, is higher than sample which, is prepared by using potassium dichromate as oxidant [23].

The infrared spectroscopic analysis of (PpCA) monomer and its analogs polymer: The IR spectra of the P-chloroaniline monomer (PCA) and its polymer (PPCA) are represented in Figure 14, while the absorption band values and their assignments are summarized in Table 5 [52-59]. The sharp absorption band appearing at 506 $cm^{-1}$ for monomer and the medium absorption band appearing at 510 $cm^{-1}$ in case of polymer may be attributed to the stretching vibration of C-Cl. The three sharp absorption bands which appear at 639, 697 and 876 $cm^{-1}$ in case of the monomer and the corresponding broad absorption bands for the polymer at 673 and 825 $cm^{-1}$ are attributed to out of plane C-H deformation for 1,4-disubstitution in benzene ring. A series of absorption bands appearing in the region from 928-1118 $cm^{-1}$ which could be attributed to out-of-plane bending of C-H bonds of aromatic ring in both cases (monomer and polymer). The sharp absorption band appearing at 1181 $cm^{-1}$ which could be attributed to stretching vibrations C-N in case of monomer, appears at 1239 $cm^{-1}$ with slightly shift in case of polymer. The shoulder and sharp absorption bands appearing at 1440 and 1494 $cm^{-1}$ in case of the monomer and the corresponding abroad absorption bands appearing at 1491 and 1509 $cm^{-1}$ in case of the polymer are attributed to stretching vibration for C=C in benzene ring of quinoid unit. The medium absorption bands appearing at 3380 $cm^{-1}$ in case of monomer which may be attributed to symmetric stretching vibrations of N-H disappear in case of polymer. The medium absorption band appearing at 3471 $cm^{-1}$ which could be attributed to asymmetric stretching vibrations for NH group in case of monomer, appears as abroad absorption band at 3485 $cm^{-1}$ in case of polymer.

**The UV-visible spectroscopic study of p-chloroaniline monomer and its analogs polymer:** The UV-visible spectra of p-chloroaniline and its polymer are represented in Figure 15; the spectra show the following absorption bands:

- In case of monomer, two absorption bands appear at $\lambda_{max}$=252 and 294 nm which may be attributed to $\pi$-$\pi^*$ transition (E2-band) of the benzene ring and the β-band (A1g-B2u) [60-62].

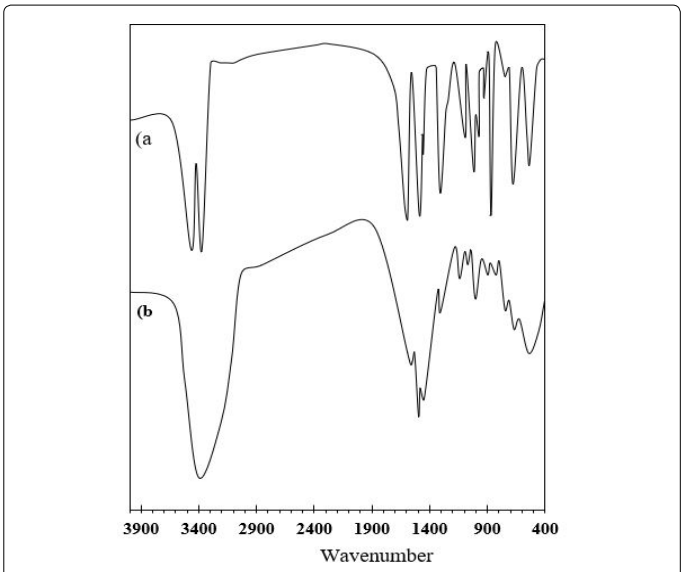


**Figure 14:** The infrared spectrum of (PCA) (a) and its analogous polymer (PpCA) (b).

| Wave number ($cm^{-1}$) | | Assignments |
|---|---|---|
| Monomer | Polymer | |
| 506 s | - | Stretching vibration of C-Cl or torsional of $NH_3$ group |
| - | 510 m | |
| 639 s | - | Out-of-plane bending deformation of CH in 1,4 disubstituted in benzene ring |
| 697 sh | - | |
| - | 673 b | |
| 823 s | - | |
| - | 825 b | |
| 876 sh | - | |
| 928s | - | Plane C-H deformation of 1,3,4-trisubistuition of benzene ring in case of polymer |
| - | 1011 b | |
| 1004 m | - | |
| 1051 sh | - | |
| 1081 s | - | |
| - | 1091 s | |
| 1118 b | - | |
| 1181 s | - | Symmetric stretching vibration of C-N group |
| - | 1172 w | |
| - | 1239 w | |
| 1288 s | - | |
| - | 1405 sh | Stretching vibration for C=C in benzene ring or C-N in quinoid unit |
| 1440 sh | - | |
| - | 1491 b | |
| 1494 s | - | |
| - | 1509 b | |
| 1616 s | - | |
| 3380 m | - | Symmetric stretching vibration of N-H |
| 3471 m | - | Asymmetric stretching vibration for NH group |
| - | 3485 b | |
| Where: S=sharp; m=medium; w=weak; b=broad; sh=shoulder. | | |

**Table 5:** Infrared absorption bands and their assignments of P-chloroaniline monomer and its analogs polymer.

• In case of polymer, the absorption band appear at $\lambda_{max}$=242 nm which may be attributed to $\pi$-$\pi^*$ transition showing a bathochromic shift. Beside this band, broad absorption band appears in the visible region at $\lambda_{max}$=432 nm which may be due to the high conjugation of the aromatic polymeric chain.

**Thermal gravimetric analysis (TGA) of poly P-chloroaniline:** Thermo-gravimetric analysis (TGA) for the prepared polymer has been investigated and the TGA-curve is represented in Figure 16. The calculated and found data for the prepared polymers is summarized in Table 6.

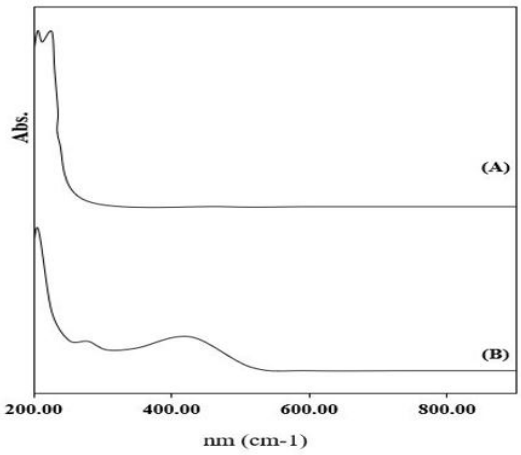


**Figure 15:** UV-visible spectra of P-chloroaniline (PCA) (A) and its analogous polymer (PpCA) (B).

The thermal degradation steps are given as follows (with Start weight 1.666 g) such as:

• The first stage includes the loss of one water molecule in the temperature range between 36-104°C the weight of loss of this step is found to be 3.08% which is in a good agreement with the calculated one (2.97%).

• The second stage, in the temperature range between 104-136°C the weight loss is found to be 6.22%, which could be attributed to the loss of one molecule of HCl. The found weight loss is in good agreement with the calculated one (6.02%).

• The third stage, in the temperature range between 136-320°C, the weight loss is found to be 23.94%, which is attributed to the loss of four molecules of Cl. The calculated weight loss of this stage is equal to 23.42%.

• The fourth stage, in the temperature range between 320-410°C, the weight loss is found to be 30.11%, which is attributed to the loss of two molecules of $C_6H_3$-NH. The calculated weight loss of this stage is equal to 29.52%.

• The fifth stage, in the temperature range between 410-454°C, the weight loss is found to be 18.40%, which is attributed to the loss of one molecule of $C_6H_3$-2NH. The calculated weight loss of this stage is equal to 17.81%.

• The last stage, above 454°C, the remained polymer molecule is found to be 18.25% including the metallic residue but the calculated one is found to be 20.27%.

**The X-ray diffraction analysis and transmission electron microscope:** The X-Ray diffraction Patterns of the prepared polymer is

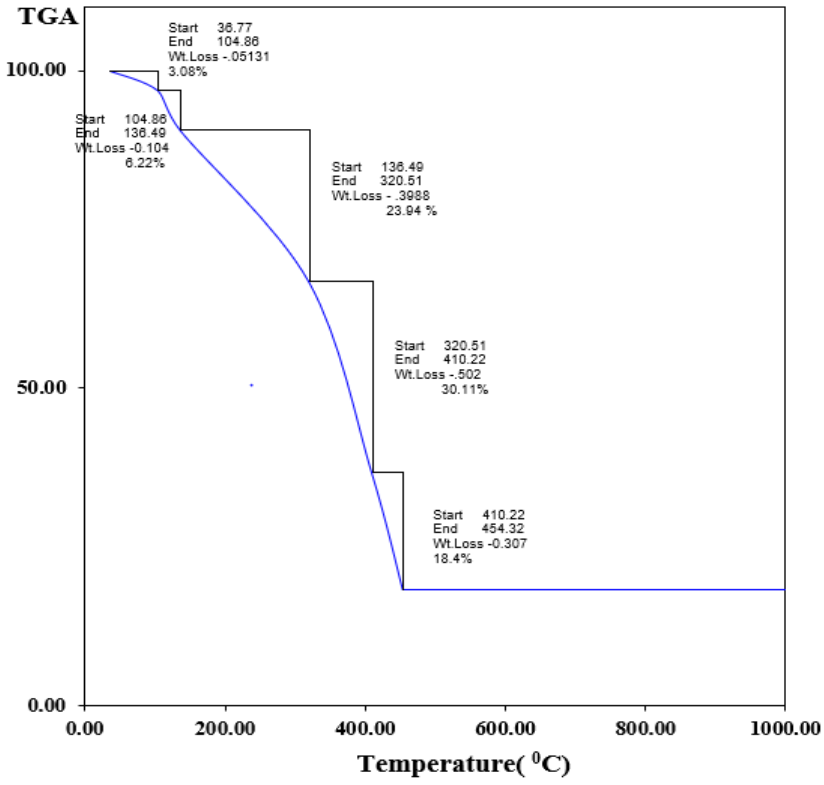


**Figure 16:** The thermal Gravimetric analysis (TGA) for the prepared polymer P-chloroaniline (PpCA).

| Name | Temperature range (°C) | Weight loss (%) | | The removed molecule |
|---|---|---|---|---|
| | | Calc. | Found | |
| Poly (PCIA) | 36.77-104.86 | 2.97 | 3.08 | $H_2O$ |
| | 104.86-136.49 | 6.02 | 6.22 | HCl |
| | 136.49-320.51 | 23.42 | 23.94 | 4Cl |
| | 320.51-410.22 | 29.52 | 30.11 | $2C_6H_3$+2NH |
| | 410.22-454.32 | 17.81 | 18.40 | $C_6H_3$+2NH |
| | Remaining weight (%) above 454.32 | 20.27 | 18.25 | Remaining weight and metallic residue |

**Table 6:** Thermogravimetric data of PpCA.

represented in Figure 17. The figure shows that, the prepared PpCA is completely amorphous.

Orphology of PpCA was characterized by transmission electron microscope. Figure 18 shows TEM image of PpCA which shows spherical irregular shape with approximate diameter 75-88 nm either separated or linked with each other.

## Dielectric properties and ac conductivity ($\sigma_{ac}$) measurements

Figure 19 show the variation in dielectric constant (έ) of PpCA as a function of frequency. From the figure it is clear that, the dielectric constant decrease sharply up to a certain frequency after which becomes nearly constant. This behavior has also been observed by Pant et al. [38-40]. This phenomenon could be attributed to relaxation process due to rotational displacement of molecular dipole under the influence of alternating filed which lead to dielectric relaxation. Consequently, decrease in dielectric constant may be due to the contribution of orientation relaxation of dipoles and conduction of charge carriers at higher frequency [41]. This can be explained on the basis of the fact that at close to high frequency, field reversal becomes so fast that dipoles are unable to orient themselves and intrawell hopping probability of charge carriers dominates in rapid field reversal in such a small interval of time [42].

Figure 20 reveals that dielectric loss ε″ decrease with increasing frequency. A decrease of ε″ orders of magnitude was observed when the frequency was increased from 0.1 kHz to 100 kHz. At low frequency, the high value of dielectric loss ε″ is usually associated with the motion of free charge carriers within the material, dipole polarization or interfacial polarization. At high frequency, periodic field reversal is so fast that there is no excess ion diffusion in the direction of electric field and thus, charge accumulates, and polarization decreases due to accumulation of charges leading to the decrease in ε″ [38-41].

Figures 21 and 22 represent the variation in ac conductivity ($\sigma_{ac}$) for (PpCA) as a function of frequency and temperature. It is observed that, the value of ac conductivity increases with the increase of frequency. This behavior is in good agreement with the random free energy model proposed [41]. According to this model, conductance increases as a function of frequency in many solids, including polymers, which can be explained on the basis of any hopping model. The rise in conductivity upon increasing the frequency and temperature is common for disordered conducting polymer. As can be seen, the curve displays a conductivity dispersion, which is strongly dependent on frequency and shows weaker temperature dependent.

The recorded conductivity value at room temperature of PpCA was found to be 0.0352 S/cm which is higher than conductivity of polyaniline-polyvinyl alcohol blends $10.5 \times 10^{-5}$ $Scm^{-1}$ and ac conductivity of HCl doped polyaniline synthesized by the interfacial polymerization technique $6.2 \times 10^{-5}$ $Scm^{-1}$. Also, the ac conductivity of PpCA is higher than polyaniline loaded with 10% molybdenum

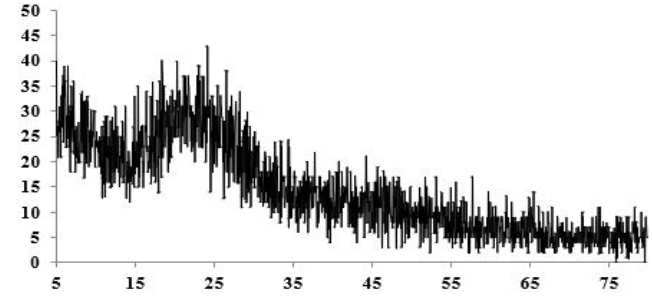


**Figure 17:** X-ray poly p-chloroaniline (PpCA).

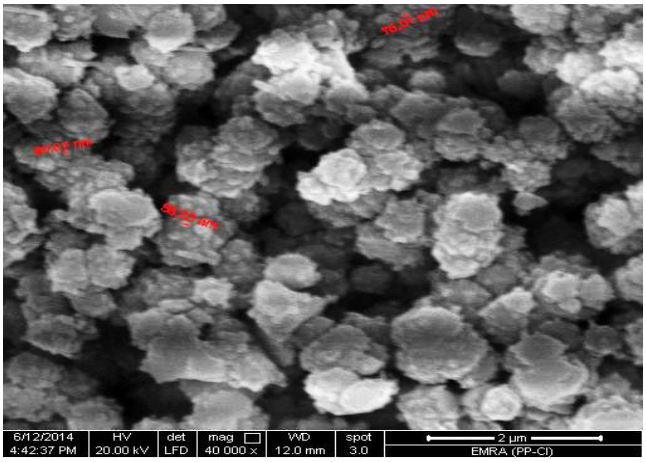


**Figure 18:** The transmission electron microscope of PpCA.

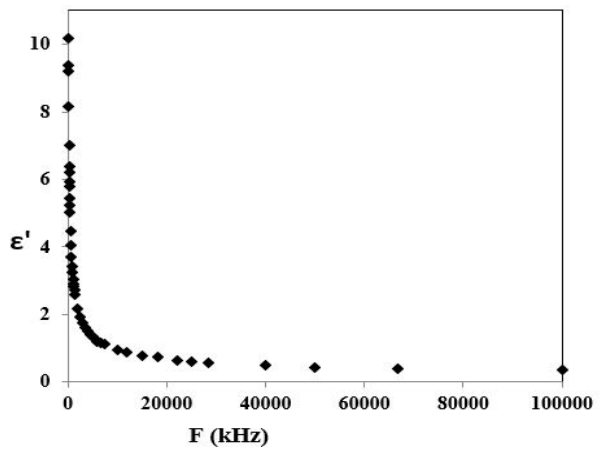


**Figure 19:** Variation of dielectric constant (έ) of (PpCA) with frequency at room temperature.

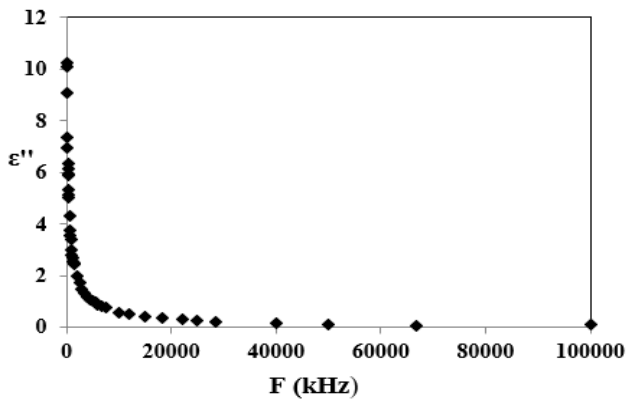


**Figure 20:** Variation of dielectric loss (ε″) of (PpCA) with frequency at room temperature.

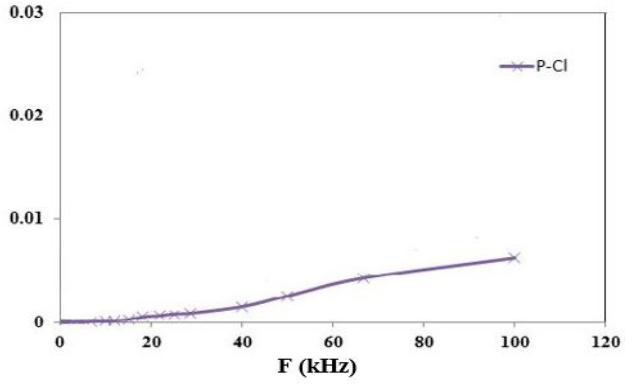


**Figure 21:** AC conductivity vs. frequency for (PpCA) at room temperature.

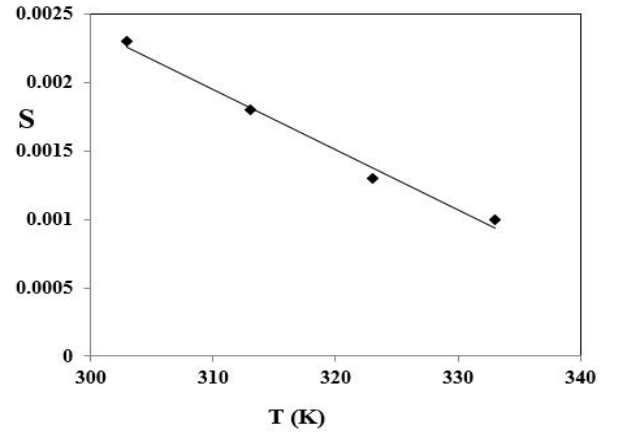


**Figure 22:** Frequency exponent (s) vs. temperature for (PpCA).

trioxide composites 0.025 s/cm but lower than the determined value of ac conductivity of polyaniline prepared by $K_2Cr_2O_7$ as oxidant 1.922 $Scm^{-1}$. Such difference could be attributed to the different disorder of each composite, substituted function group and using of different dopant.

In general, for amorphous conducting material, disordered systems, low mobility polymers and even crystalline materials, the ac conductivity ($\sigma_{ac}$) as a function of frequency can be obeys a power law with frequency [40-42,63-66]. The ac conductivity ($\sigma_{ac}$) over a wide range of frequencies can be expressed as: $\sigma_{ac}(\omega)=A\omega s$ (20), where A is a complex constant and the index (s) is frequency exponent and ω is the angular frequency ($\omega=2\pi f$).

Figure 23 shows the relation between Ln $\sigma_{ac}$ and Ln ω at different temperatures. The value of (s) at each temperature has been calculated from the slope of ln σ (ω) versus ln (ω) plot. As shown in Figure 21 the calculated value of (s) for (PpCA) sample is less than unity. The microscopic conduction mechanism of disordered systems is governed by two physical processes such as classical hopping or quantum mechanical tunneling of charge carries over the potential barrier separating two energetically favorable centers in a random distribution. The exact nature of charge transport is mainly obtained experimentally from the temperature variation of exponent (s) [43]. The temperature exponent (s) dependences for (PPCA) sample reveals that the frequency exponent (s) decreases with the increase of temperature. This behavior is only observed in the correlated barrier hopping model proposed by Elliott [44].

## DFT calculations

From the polymerization mechanism in Section 6.4, the radical cation formed in the initial step (0-5 min) followed by the propagation step involves the interaction between the formed radical cation and the neutral monomer to form a dimer radical cation. The From the polymerization mechanism, the radical cation formed in the initial step dimer radical cation interacts with another neutral monomer to form trimmer radical cation and so on to form the polymer chain. In this section, using theoretical calculation to explore why radical cation starts the polymerization and not the neutral monomer of p-chloroaniline and at formation and the stability of the dimer radical cation (ortho-attack) or (meta-attack) in the propagation steps.

**Monomer and radical cation (Initiation):** The final optimized geometry, the vector of the dipole moment, and HOMO charge density maps of monomer neutral and radical cation PpCA using DFT-B3LYP/6-311G** are presented in Figures 24 and 25. The energetics of monomer and radical cation are listed in Table 7. From the data in Figures 24 and 25 and Table 7 the computed Eg (energy gap) of the radical cation is less than the Eg of the netral monomer by 6.15 eV (73 kcal). As the energy gap of the molecule decreases, the reactivity increases. The reason why radical cation is more reactive and starting the process of polymerization. The natural charge of N-atom of amino

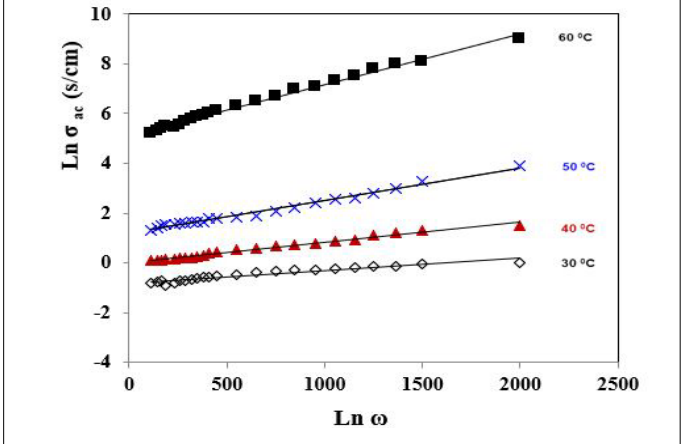


**Figure 23:** Ac conductivity vs. angular frequency for (PpCA) with frequency at different temperatures.

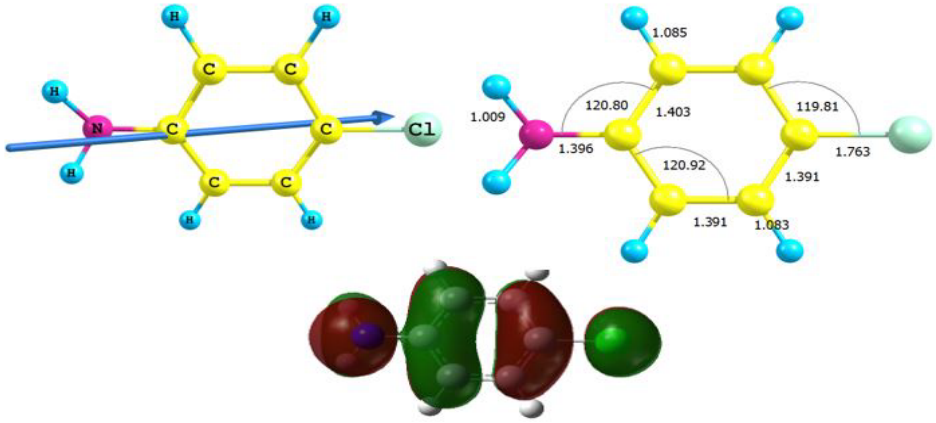


**Figure 24:** Geometry optimization, numbering system, vector dipole moment, bond length, net charge and HOMO charge density of the monomer (PCA).

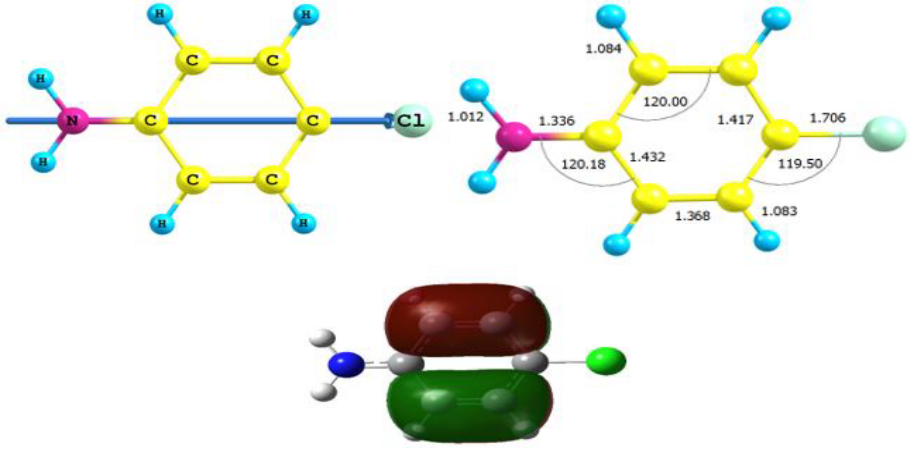


**Figure 25:** Geometry optimization, numbering system, vector dipole moment, bond length, net charge and HOMO charge density of (PCA) radical cation.

group in the neutral monomer is -0.7894 e whereas, in monomer radical cation is -0.5893 e and in dimer radical cation is -0.591 e. The decreases in the natural charge on N-atom of $NH_2^+$ is another reason for why this group attack the ortho- or meta-position of the neutral monomer to start the polymerization process.

**Some general remarks can be considered**

- The computed total energy of radical cation is less stable then neutral monomer by 8.109 eV (186.998 Kcal), indicating that the radical cation is more reaction than neutral monomer.
- The computed energy gap (Eg), which measure the reactivity. As the energy gap decrease the reactivity increase. In our case the Eg of radical cation is less than the neutral monomer by 3.150 eV (72.629 Kcal), this a second reason why radical cation is more reactive and starting the process of polymerization.
- From the computed dipole moment, it is found that the dipole moment of radical cation is greater than the neutral monomer by 3.02 D.
- The net charge on N-atom of amino group in neutral monomer is -0.311 e whereas, in radical cation is -0.198 e. The decrease in negativity of N-atom of amino group is another reason for this center to attack the ortho- or meta position of the neutral monomer to start polymerization as indicated in HOMO charge density map (Figures 24 and 25).

| Parameter | Monomer | Radical cation |
|---|---|---|
| $E_T$ (a.u) | -747.3 | -747 |
| $E_{HOMO}$ (a.u) | -0.217 | -0.415 |
| $E_{LUMO}$ (a.u) | -0.028 | -0.341 |
| $E_g$ (eV) | 5.1566 | 2.0071 |
| Total μ | 3.44 | 6.46 |

**Table 7:** The total energy, energy of HOMO and LUMO, energy gap and vector of the dipole moment of the monomer and the radical cation of (PTO).

**Propagation step:** The next step of the polymerization is the propagation step at which the radical cation attacks another monomer to form the dimer radical cation.

To prove which position in the monomer attack by the radical cation to form the dimer radical cation is to calculate the total energy of the dimer radical cation at B3LYP/ 6-311G** method. Figures 26 and 27 present the final geometry, the vector of the dipole moment, total

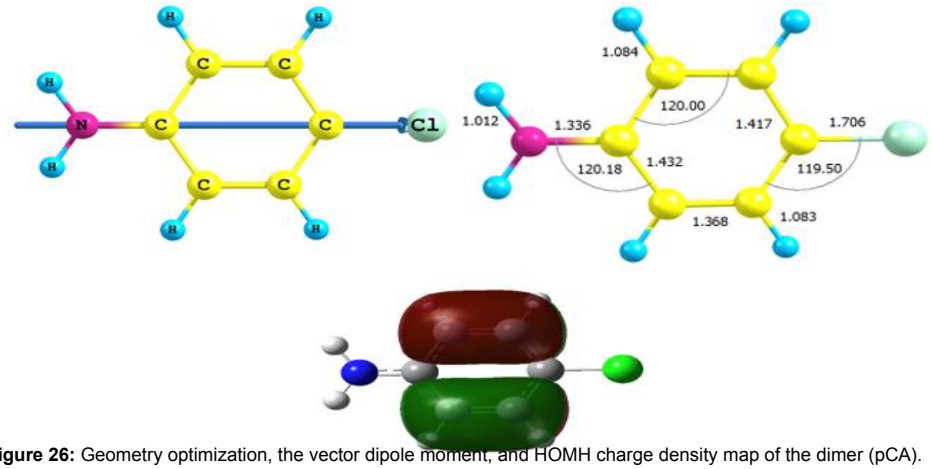


**Figure 26:** Geometry optimization, the vector dipole moment, and HOMH charge density map of the dimer (pCA).

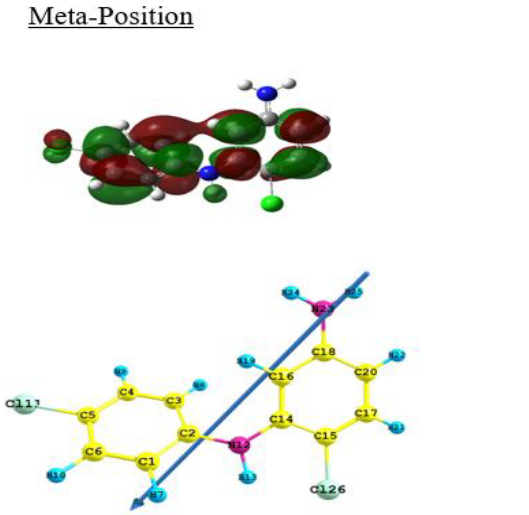


**Figure 27:** Geometry optimization, the vector dipole moment, and HOMO charge density map of the dimer (pCA).

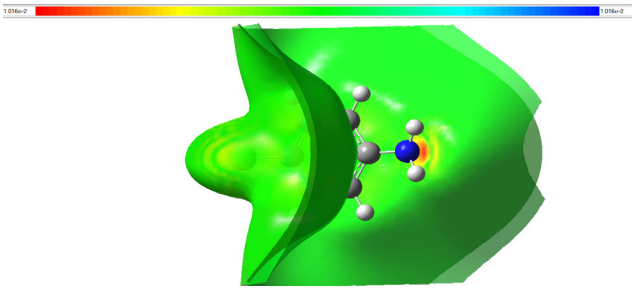

**Figure 28:** Electrostatic potential from total SCF density of monomer.

energy and energy gap and HOMO charge density maps to two possible structures. Two possible structures may be considered, dimer radical cation (ortho- attack) and dimer radical cation (meta-attack). From Figures 26 and 27 one can reveal the following:

• The computed total energy (which measure the stability of any compound) of dimer radical cation (meta-attack) is less (more stable) than dimer radical cation (ortho-attack) by 5.77 eV (133 kcal). This means that in the reaction medium dimer radical cation (meta-attack) is a predominant than dimer radical cation (ortho-attack).

• Another reason why dimer radical cation (meta-attack) is more reactive than (ortho-attack) is the energy gap, as the energy gap decrease, the reactivity increase. Dimer radical cation (meta-attack) is more reactive than dimer radical cation (ortho-attack) by 0.323 eV (7.4 kcal). From the above, one concludes that in the initiation process, the radical cation is more stable than monomer and dimer radical cation (meta-attack) is more stable than dimer radical cation (ortho-attack) in the propagation process (Figures 28 and 29).

dimer radical cation (meta-attack) interacts with another monomer to form trimmer radical cation. We have two probabilities I (meta-attach) and II (ortho-attach) as in Figure 30. We calculate the total energy and energy gap we find that, the trimmer (meta-attach) (Figure 31), is more stable than trimmer (ortho-attack) by ~ 200 kcal) and energy gap is the same for I and II. This means that in the reaction medium trimmer (meta- attack) is a predominant than trimmer (ortho-attack). Similarly, we find that the tetramer (meta-attack) (Figure 32) more stable than tetramer (ortho-attack) and so on to form polymer chain (Scheme 2).

**Global reactivity descriptors:** They include HOMO, LUMO, energy gap (Eg), chemical hardne (η), electronegativity (X), chemical potential (V), electron affinity (A), ionization potential (I) and chemical softness (S) which are calculated at B3LYP/6-311G**.

The frontier molecular orbital (FMO) energies of the studied compounds were calculated using B3LYP/6-311G**. HOMO energy characterizes the electron donating ability, while LUMO energy characterizes the electron withdrawing ability. Energy gap ($E_g$) between HOMO and LUMO characterizes the molecular chemical stability which is a critical parameter in determining molecular electrical transport properties because it is a measure of electron conductivity.

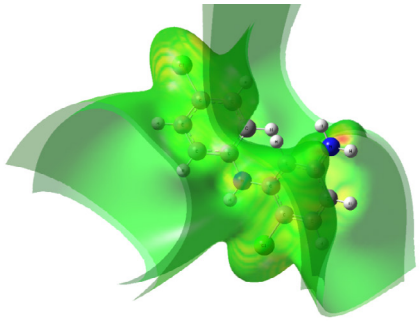

**Figure 29:** Electrostatic potential from total SCF density of m-dimer.

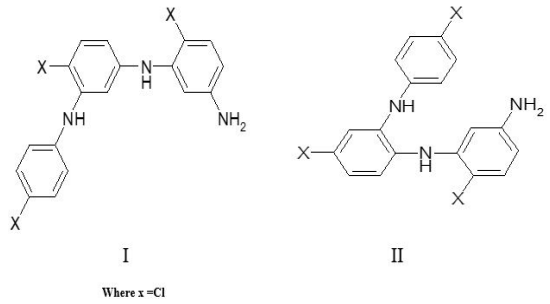


**Figure 30:** I represent meta-attach and II represent ortho-attach.

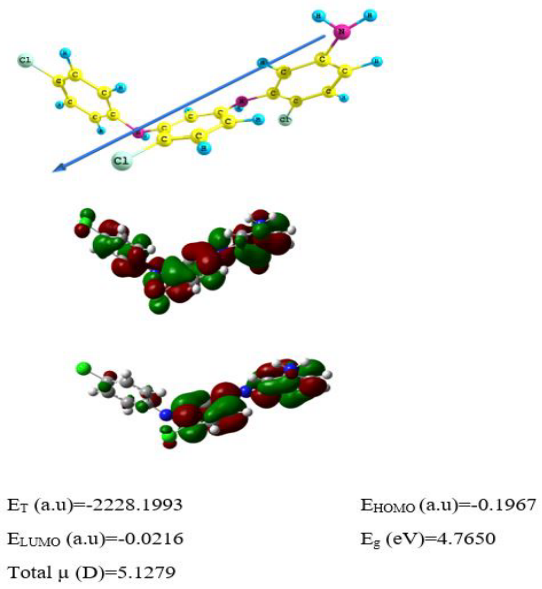


**Figure 31:** Geometry optimization, the vector dipole moment, charge density maps of the HOMO and LUMO for the trimmer (meta- attack) (PCIA).

The results in Figure 28 and Table 8, indicate that the smaller the energy gap the easier the charge transfer and the polarization occurs within the molecule. Furthermore, the order of increasing reactivity is: $D^+ > M^+ > M$ (where $D^+$ is dimer radical cation, $M^+$ is monomer radical cation and M neutral monomer). Using HOMO and LUMO energies, ionization potential and electron affinity can be expressed as I ~ -EHOMO, A ~ -ELUMO at the RHF/ 6-311G** as shown in Table 8. The variation of electronegativity (X) values is supported by electrostatic potential, for any two molecules, where electron will be partially transferred from one of low X to that of high X. The results show that the order of decreasing X is: $M^+ > MD^+$.

The chemical hardness (η)=(I-A)/2, electronegativity(X)=(I+A)/2, chemical potential (V)=-(I+E)/2 and chemical softness (S)=1/2η values are calculated and presented in Table 8. The results of small η values for the studied compounds reflect the ability of charge transfer inside the molecule. Therefore, the order is: $M > D^+ > M^+$.

**Non-linear optical properties (NLO):** So far, no experimental or theoretical investigations were found addressing NLO for these classes of molecules; therefore, this triggered our interest to undertake this study. NLO is at the forefront of current research due to its importance in providing key functions of frequency shifting, optical modulation, switching, laser, fiber, optical materials logic and optical memory for the emerging technologies in areas such as telecommunications, signal processing and optical inter connections [45,46]. In order to investigate the relationship between molecular structure and NLO, the polarizabilities and hyperpolarizabilities of the studied M, $M^+$ and $D^+$ are calculated using B3LYP/6-311G** [52-56]. Total static dipole moment (μ), the mean polarizibility α, the anisotropy of the polarizability Δα and the mean first-order hyperpolarizibility (β) are listed in Table 9. The polarizabilities and first-order hyperpolarizabilities are reported in atomic units (a.u.), the calculated values have been converted into electrostatic units (esu) using conversion factor of $0.1482 \times 10^{-24}$ esu for α and $8.6393 \times 10^{-33}$ esu for β. P-nitro aniline (PNA) is a standard prototype used in NLO studies. In this study, PNA is chosen as a reference as there were no experimental values of NLO properties of the studied molecules. The magnitude of the molecular hyperpolarizability β is one of the key factors in NLO system. The analysis of the β parameter show that the monomer PpCA is three times greater than PNA, $M^+$ is 12 times greater than PNA and $D^+$ is 7 times greater than PNA. The large value of the β parameter for M, $M^+$ and $D^+$ implying their promising applications as NLO materials.

**Molecular electrostatic potential (MEP):** Molecular electrostatic potential (MEP) is related to the electronic density and is a very useful descriptor in understanding sites for electrophilic and nucleophilic attack as well as hydrogen bonding interactions [47,48]. This is correlated with dipole moments, electronegativity, partial charges and chemical reactivity of the molecules. These maps allow us to visualize variably charged regions of a molecule. Knowledge of the charge distributions can be used to determine how molecules interact with one another. The calculated 3D MEP of monomer and dimer cation (m-attack) molecules are calculated from optimized molecular structure using B3LYP/6-311G** are shown in Figures 28 and 29. The results show that, in case of neutral monomer the negative region (red) is mainly over the N atomic site, which is caused by the contribution of lone-pair electrons of nitrogen atom while the positive (blue) potential sites are around the hydrogen and carbon atoms. Also, in case of dimer radical cation, the

| Parameters | Mon | Cat | DI |
|---|---|---|---|
| IP | 5.906 | 11.294 | 5.3133 |
| EA | 0.7494 | 9.2868 | 0.4955 |
| $\eta$ | 2.5783 | 1.0036 | 2.4089 |
| $\chi$ | 3.3277 | 10.29 | 2.9044 |
| V | -3.328 | -10.29 | -2.904 |
| S | 1.2892 | 0.5018 | 1.2045 |

**Table 8:** The ionization potential (I/eV), electron affinity (A/eV), chemical hardness (η/ eV), softness (S/$eV^{-1}$), chemical potential (V) and electronegativity (χ/eV), for monomer, radical cation and dimer of p- chloro aniline using B3LYP/6-311G (d,P).

| Property | PNA | Monemer | Cation | Dimer | |
|---|---|---|---|---|---|
| | | B3LYP/6-311G(d,P) | B3LYP/6-311G(d,P) | B3LYP/6-311G(d,P) | Unit |
| μx | 2.44 Debye[a] | 3.3086 | 6.4609 | 2.5987 | Debye |
| μy | | 0 | -0.0001 | 3.1598 | Debye |
| μz | | 0.9437 | 0.0005 | 0.9974 | Debye |
| μ | | 3.4406 | 6.4609 | 4.211 | Debye |
| αXX | $22 \times 10^{-24}$ cm[3b] | -49.539 | 20.2552 | -115.558 | a.u |
| αXY | | 0 | -0.0002 | 14.9955 | a.u |
| αYY | | -47.5187 | -2.0808 | -90.9218 | a.u |
| αZZ | | -58.9068 | -18.1743 | -110.61 | a.u |
| αYZ | | 0 | 0.0002 | -3.5783 | a.u |
| αXZ | | 3.9873 | 0.0016 | -1.7262 | a.u |
| <α> | | $-51.99 \times 10^{-24}$ | 0 | $-105.69 \times 10^{-24}$ | esu |
| Δα | | $10.524 \times 10^{-24}$ | $33.427 \times 10^{-24}$ | $-22.571 \times 10^{-24}$ | esu |
| βxxx | $15.5 \times 10^{-30}$ esu[c] | 39.1235 | 87.4274 | 135.3211 | a.u |
| βxxy | | 0 | 0 | 31.9684 | a.u |
| βxyy | | 7.2922 | 12.6542 | 22.5452 | a.u |
| βyyy | | 0 | 0 | 64.8238 | a.u |
| βxxz | | 15.6308 | 0.0103 | 3.7713 | a.u |
| βxyz | | 0 | 0 | 14.1829 | a.u |
| βyyz | | 0.5411 | 0 | 15.3853 | a.u |
| βxzz | | -5.5261 | -4.0371 | -13.4228 | a.u |
| βyzz | | 0 | 0 | -3.2765 | a.u |
| βzzz | | 0.6638 | 0.0015 | -1.4477 | a.u |
| <β> | | $44.22 \times 10^{-30}$ | $172.98 \times 10^{-30}$ | $99.04 \times 10^{-30}$ | esu |

**Table 9:** Total static dipol moment (μ), the mean polarizability (<α>), the anisotropy of the polarizability (Δα), and the mean first-order hyperpolarizability (<β>) for monomer, radical cation and dimer of p-chloro aniline using B3LYP/6-311G(d,P).

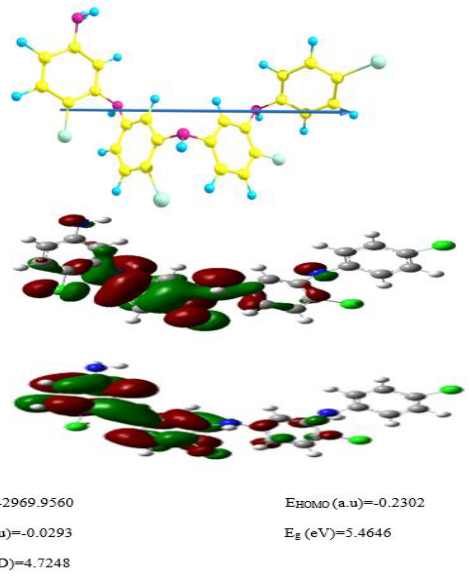


**Figure 32:** Geometry optimization, the vector dipole moment, charge density maps of the HOMO and LUMO for P-Cl aniline oligomers.

negative red region is mainly over the terminal N-atom. A portion of the molecule that has negative electrostatic potential will be susceptible to electrophilic attack-the more negative the higher the tendency for electrophilic attack.

## Conclusions

In the present work PpCA polymer was synthesized with potassium dichromate as initiator in the presence of HCl. The optimum yield formation of PpCA is obtained at 0.3 M potassium dichromate 0.2 M of the monomer and 0.5 M hydrochloric acid concentrations. The kinetics of the oxidative chemical polymerization using potassium dichromate as oxidant for p-chloroaniline monomer in aqueous HCl medium was done. The initial and overall rate of polymerization reaction increases with increasing the oxidant, monomer, and HCl concentrations. The exponent of oxidant, monomer, and HCl was found to be 0.934, 1.142, and 1.017 respectively. The obtained polymer was characterized by IR, UV-visible, TGA, elemental analysis, X-ray, transmission electron microscopy (TEM). The chrome is present between polymer chains as sandwich-bonded $C_6H$-$C_6H_6$ groups and the usual formation procedure hydrolyzes the reaction mixture with dilute acid which gives the cation $(C_6H_6)$ $2Cr^{3+}$. The a.c conductivity increases with the increase of frequency and temperature. The microscopic conduction mechanism of charge which carries over the potential barrier in polymer backbone is classical hopping model. The mechanism of the polymerization process was investigated theoretically using DFT-B3LYP/6-311G** and we proved theoretically that in the polymerization reaction (in Propagation step) the attack was started and continued in meta-position and not ortho-position or para position. The electronic dipole moment (μ) and first order hyperpolarizability (β) values of the monomer, radical cation and dimer cation have been computed to study the NLO properties. Finally, global reactivity descriptors including electronegativity (X), hardness (η), softness (S) of the monomer, radical cation and dimer cation were calculated and analyzed, while molecular electrostatic potential (MEP) of some selected molecules were explored as well.

### References

1. Hirase R, Shikata T, Shirai M (2004) Selective formation of polyaniline on wool by chemical polymerization, using potassium iodate. Synth Met 146: 73..
2. Ju Q, Shi Y (2013) Performance study of magnesium-polyaniline rechargeable

battery in 1-ethyl-3-methylimidazoliumethyl sulfate electrolyte. Synth Met 178: 27-33.

3. Steffens C, Manzoli A, Oliveira JE, Leite FL, Correa DS, et al. (2014) Bio-inspired sensor for insect pheromone analysis based on polyaniline functionalized AFM cantilever sensor. Sens Actuators B Chem 191: 643-649.
4. Wang L, Hua E, Liang M (2014) Graphene sheets, polyaniline and AuNPs based DNA sensor for electrochemical determination of BCR/ABL fusion gene with functional hairpin probe. Biosensors and Bioelectronics 51: 201-207.
5. Talwar V, Singh O, Singh R (2014) ZnO assisted polyaniline nanofibers and its application as ammonia gas sensor. Sensors and Actuators B 191: 276-282.
6. Moon Y, Yun J, Kim H (2013) Synergetic improvement in electromagnetic interference shielding characteristics of polyaniline-coated graphite oxide/gamma-Fe2O3/BaTiO3 nanocomposites. Journal of Industrial and Engineering Chemistry 19: 493-497.
7. Gupta G, Birbilis N, Cook AB, Khanna AS (2013) Polyaniline-lignosulfonate/epoxy coating for corrosion protection of AA2024-T3. Corrosion Science 67: 256-267.
8. Karthikaiselvi R, Subhashini S (2013) Study of adsorption properties and inhibition of mild steel corrosion in hydrochloric acid media by water soluble composite poly (vinyl alcohol-omethoxy aniline). Journal of the Association of Arab Universities for Basic and Applied Sciences.
9. Martin X, Mullen K (2013) Designing p-conjugated polymers for organic electronics. Progress in Polymer Science 38: 1832-1908.
10. Gopodinova K, Terlemezyan L (1998) Conducting polymers prepared by oxidative polymerization: polyaniline. Progress in Polymer Science 23: 1443-1484.
11. Gurunathan K, Murugan AV, Marimuthu R, Mulik UP, Amalnerkar DP (1999) Electrochemically synthesised conducting polymeric materials for applications towards technology in electronics, optoelectronics and energy storage devices. Progress in Polymer Science 23: 1443-1484.
12. Balakrishna P, Murty BN, Yadav RB, Anuradha M, Narayanan PSA, et al. (2010) Admixed binders and lubricants in ceramic powder pressing-A study of zinc behenate additive. IJEMS 5: 136-139.
13. Meirong H (2008) Synthesis and Application of Functional Polychloroanilines. J Tong Uni 34: 1079-1083.
14. Xu G, Hai-Chao G, Zheng-Fei MA, Xiao-Qin L (2010) Calculations of density functional theory based on orientation effect of polychloroaniline on electrophilic substitution. J Nan Uni Tech.
15. Sayyah SM, Abd El-Salam HM, Azzam EMS (2005) Surface activity of monomeric and polymeric (3-alkyloxy aniline) surfactants. Int J Pol Mat 54: 541-555.
16. Sayyah SM, Abd El-Khalek AA, Bahgat AA, Abd El-Salam HA (2001) Kinetic studies of the chemical polymerization of substituted aniline in aqueous solutions and characterization of the polymer obtained Part 1.3- Chloroaniline. Pol Int 50: 197-206.
17. Sayyah SM, Bahgat AA, Abd El-Salam HM (2002) Kinetic studies of the aqueous oxidative polymerization of 3- hydroxyaniline and characterization of the polymer obtained. Int J Pol Mat 51: 291-314.
18. Sayyah SM, Abd El-Salam HM (2003) Aqueous oxidative polymerization of N methyle aniline in acid medium and characterization of the obtained polymer. International J Pol Mat 52: 1087-1111.
19. Sayyah SM, Abd El-Khalek AA, Bahgat AA, Abd El-Salam HM (2001) Kinetic studies of the polymerization of substituted aniline in aqueous solutions and characterization of the polymer obtained. Part 2. 3- methylaniline. Int J Pol Mat 49: 25-49.
20. Sayyah SM, Abd El-Salam HM, Bahgat AA (2002) Aqueous oxidative polymerization of 3-methoxyaniline and characterization of its polymer. Int J Pol Mat 51: 915-938.
21. Sayyah SM, Bahgat AA, Abd El-Salam HM (2002) Kinetic studies of the aqueous oxidative polymerization of 3-hydroxyaniline and characterization of the polymer obtained. Int J Pol Mat 51: 291-314.
22. Sayyah SM, Aboud AA, Mohamed SM (2014) Chemical Polymerization Kinetics of Poly-O-Phenylenediamine and Characterization of the Obtained Polymer in Aqueous Hydrochloric Acid Solution Using $K_2Cr_2O_7$ as Oxidizing Agent. Int J Pol Sci.
23. Sayyah SM, Amgad A, Khaliel B, Salama M (2014) Oxidative Chemical Polymerization of Ortho-Tolidine in Acid Medium Using $K_2Cr_2O_7$ as Oxidizing Agent and Characterization of the Obtained Polymer. Int J Adv Res 2: 586-607.
24. Frisch GW, Schlegel HB, Scuseria GE, Robb MA, Cheeseman JR, et al. (2009) Electronic Supplementary Material (ESI) for Chemical Science. The Royal Society of Chemistry.
25. Schaefer T, Wildman TA, Salman SR (1980) The perpendicular conformation of 2-hydroxythiophenol. Intramolecular hydrogen bonding to a specific lone pair. J Am Chem Soc 102: 107-110.
26. Schaefer T, Salman SR, Wildman TA, Clark PD (1982) Conformational consequences of intramolecular hydrogen bonding by OH to the directional lone-pair of sulfur in derivatives of methyl phenyl sulfide, diphenyl sulfide, and diphenyl disulfide. Can J Chem 60: 342-348.
27. Becke AD (1993) Density-functional thermochemistry III. The role of exact exchange. J Chem Phys 98: 5648.
28. Ulic SE, Védova COD, Hermann A, Mack HG, Oberhammer H (2008) Preparation and Properties of Trifluorothioacetic Acid- S-(trifluoromethyl)ester, CF3C(O)SCF3. J Phys Chem A 112: 6211-6216.
29. Reed AE, Weinhold F (1983) Natural bond orbital analysis of near-Hartree–Fock water dimer. J Chem Phys 78: 4066.
30. Pearson RG (1986) Absolute electronegativity and Hardness correlated with molecular orbital theory. Proceeding of the National Academy of Science 83: 8440-8441.
31. Chandra AK, Uchimara T (2001) Hardness profile: a critical study. J Phy Chem A 105: 3578-3582.
32. Chen X, Yan F, Wu M, Tian HB, Li SX (2016) High Resolution Electron Momentum Spectroscopy Study on Ethanol: Orbital Electron Momentum Distributions for Individual Conformers. Chem Phys Lett 472: 19.
33. Avci D (2011) Second and third-order nonlinear optical properties and molecular parameters of azo chromophores: semiemperical. Spectrochimica Acta A 82: 37-43.
34. Avci D, Başoğlu A, Atalay Y (2010) Ab-initio HF and DFT calculations on an organic nonlinear optical material. Str Chem 21: 213-219.
35. Avci D, Cömert H, Atalay Y (2008) Ab-initio Hartree-Fock calculations on linear and second-order nonlinear optical properties of new acridine-benzothiazolylamine chromophores. J Mol Mod 14: 161-169.
36. Chowdhury P, Saha B (2005) Potassium dichromate-initiated polymerization of aniline. Ind J Chem Tech 12: 671-675.
37. Sayyah SM, Abed El-Salam HM, Azzam EMS (2006) Oxidative Chemical Polymerization of Some 3-alkyloxyaniline Surfactants and Characterization of the Obtained Polymers. Int J Pol Mat 55: 1075-1093.
38. Pant HC, Patra MK, Negi SC, Bhatia A, Vadera SR, et al. (2006) Studies on conductivity and dielectric properties of polyanilinezinc sulphide composites. Bull Mater Sci 29: 379.
39. Dyre JC (1988) The random free energy barrier model for ac conduction in disordered solids. J Appl Phys 64: 2456.
40. Tomara AK, Suman M, Rishi PC, Shyam K (2012) Structural and dielectric spectroscopic studies of polyaniline-poly (methyl-methacrylate) composite films. Synth Met 162: 820-826.
41. Mardare D, Rusu GI, Optoelectron J (2004) Comparison of the dielectric properties for doped and undoped TIO2 thin film. Adv Mater 6: 333-336.
42. Paphanassiou A (2002) The power law dependence of the a.c. conductivity on frequency in amorphous solids. J Phys D Applied Phys 35: 17.
43. Dey A, De S, De A, De SK (2004) Characterization and dielectric properties of polyaniline-TiO2 nanocomposites. Nanotech 15: 1277-1283.
44. Elliott S (1987) Ac Conduction in amorphous chalcogenide and pnictide semiconductors. Adv Phys 37: 135.
45. Natorajan S, Shanmugam G, Martin SA (2008) Design and nonlinear optical properties (NLO) using DFT approach of new Cr(III), VO(II), and Ni(II) chelates incorporating tri-dentate imine ligand for DNA interaction, antimicrobial,

anticancer activities and molecular docking studies. Cryst Res Technol 43: 561-564.

46. Chemia DS, Zysss J (1987) Nonlinear Optical Properties of Organic Molecules and Crystals. Academic Press, USA.

47. Bradshow DS, Andrews DL (2009) Quantum channels in nonlinear optical processes. J Nonlinear Opt Phys Matter 18: 285-299.

48. De Dominicis L, Fantoni R (2006) Symmetry Based Approach to the Evaluation of Second Order NLO Properties of Carbon Nanotubes. Non-Linear Opt Pro Mat, pp: 319-335.

49. Tang G, Zhao J, Jiang Z, Kou S, Wei C, et al. (2012) DFT and ab initio study on non-linear optical (NLO) properties of some organic complexes with different conjugate linker and substituent groups. Opt Spectr 113: 240-258.

50. Soliman S, Massoud RA, Hagar ME (2015) DFT Studies on Factors Affecting Non-Linear Optical Properties of N-Salicylidene-Chloroaniline Schiff Bases. Asian J Chem 27: 3481-3483.

51. Vijayalakshmi S, Kalyanaraman S (2015) Analysis on linear and nonlinear optical properties of two Bisphenols with DFT approach: A comparative study. Opt Mat 42: 215-219.

52. Abeyasinghe N, de Silva R, Nalin KM, De S, Silva K (2016) Non-linear Optical (NLO) Properties of Conjugated Thiophene and Ethylene Dioxy Thiophene (EDOT) Oligomers: A Density Functional Theory (DFT) Study. Int Res J Pure Appl Chem.

53. Samir AAL, Moustafa H (2017) Synthesis, characterization, electronic structure, and non-linear optical properties (NLO) of Mn (II), Co (II), Ni (II), Cu (II) and Zn (II) complexes with 5-phenylazo-8-hydroxyquinoline using DFT approach. Appl Organ Chem 1: 31-40.

54. Moustafa H, Elshakre ME, Elramly S (2017) Electronic structure and nonlinear optical properties (NLO) of 2,4-di-aryl-1,5-benzothiazepine derivatives using DFT approach. J Mol Stru 1136: 25-36.

55. Loai A, Nuha A (2018) Flame Propagation Model and Combustion Phenomena: Observations, Characteristics, Investigations, Technical Indicators, and Mechanisms. J Ener Cons 1: 31.

56. Halim SA, Omima MI (2018) DFT Calculations, Spectroscopic Studies, Biological Activity and Non Linear Optical Properties (NLO) of Novel Ternary Cu(II)-Chelates Derived from 5-Acetyl-4-hydroxy-2H-1,3-thiazinedione. Applied Organo Chem 32: 4435.

57. Rajeshirke M, Sekar N (2018) Optical Materials NLO properties of ester containing fluorescent carbazole based styryl dyes Consolidated spectroscopic and DFT approach. Opt Mat 76: 191-209.

58. Murray JS, Sen K (1996) Molecular Electrostatic Potentials, Concepts and Applications. Elsevier, Amsterdam, Netherlands, pp: 7-624.

59. Scrocco E, Tomasi J (1978) Electronic Molecular Structure, Reactivity and Intermolecular Forces: An Euristic Interpretation by Means of Electrostatic Molecular Potentials. Adv Quant Chem 11: 115-121.

60. Field LD, Sternhell S, Kalman JR (2008) Organic Structures from Spectra. 4th edn. John Wiley and Sons Ltd.

61. Tony O (1996) Fundamentals of UV-visible spectroscopy. Hewlett-Packard Publication Number 12: 5965-5123.

62. Subodh K (2006) Spectroscopy of Organic Compounds. Dept of Chemistry, Guru Nanak Dev University, Amritsar.

63. Davide F (2014) UV-Vis spectroscopy. Paul Scherrer Institute.

64. Oleksiy SJ, Prokeš IK, Stejskal J (2002) AC conductivity in aniline-1,4-phenylenediamine copolymers. Mol Crys Liq Crys 385:33-42.

65. Khalid M, Mohammad F (2007) Preparation, electrical properties and thermal stability of conductive polyaniline: nylon-6,6 composite films. eXP Poly Lett 11: 711-716.

66. Ahmed AA, Mohammad F (2006) Studies on electrically conducting polyaniline: nylon-6,6 composites: A potential material for electrical and electronic applications. J Solid-State Phe 111: 95-98.